Since January 2020 Elsevier has created a COVID-19 resource centre with free information in English and Mandarin on the novel coronavirus COVID-19. The COVID-19 resource centre is hosted on Elsevier Connect, the company's public news and information website.

Science of the Total Environment 770 (2021) 144725

Contents lists available at ScienceDirect

Science of the Total Environment

journal homepage: www.elsevier.com/locate/scitotenv

Onsite real-time detection of covid-like-virus transmission through air using spark-induced plasma spectroscopy

Jun-Ho Yang [a], Jaehun Jung [b], Seonghwan Kim [c], Youngkyu Cho [c], Jack J. Yoh [a,*]

[a] Department of Mechanical & Aerospace Engineering, Seoul National University, 1 Gwanakro, Gwanakgu, Seoul 151-742, Republic of Korea
[b] Department of Aerospace System Engineering, Seoul National University, 1 Gwanakro, Gwanakgu, Seoul 151-742, Republic of Korea
[c] Sensor Lab, Smart Device Team, Samsung Research, Samsung Electronics Co., LTD, Seoul R&D Campus, Umyeon-dong 33, Seongchon-gil, Secho-gu, Seoul 06765, Republic of Korea

HIGHLIGHTS

- We performed real-time detection of virus propagation using SIPS.
- Density of virus floating at different spray distance and time was measured.
- The droplet propagation decreased with propagation time and distance.
- The study enabled instantaneous monitoring of coronavirus present in the air.

GRAPHICAL ABSTRACT

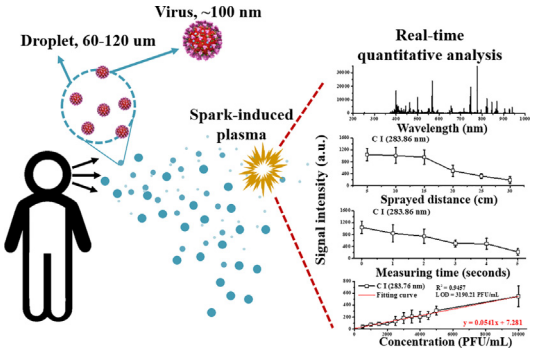

ARTICLE INFO

Article history:
Received 17 November 2020
Received in revised form 16 December 2020
Accepted 23 December 2020
Available online 23 January 2021

Editor: Jianmin Chen

Keywords:
Virus
Airborne transmission
Spark-induced plasma spectroscopy (SIPS)
Real-time analysis
Sprayed distance
Measuring time

ABSTRACT

In March 2020, COVID-19 was officially classified as a pandemic and as a consequence people have adopted strenuous measures to prevent infection, such as the wearing of PPE and self-quarantining, with no knowledge of when the measures will no longer be necessary. Coronavirus has long been known to be non-infectious when airborne; however, studies are starting to show that the virus can infect through airborne transmission and can remain airborne for a significant period of time. In the present study, a spark-induced plasma spectroscopy was devised to characterize the air propagation of the virus in real-time. The risk of air propagation was evaluated in terms of changes in virus concentration with respect to distance traveled and measurement time. Thus, our study provides a benchmark for performing real-time detection of virus propagation and instantaneous monitoring of coronavirus in the air.

1. Introduction

Scientists have recently discovered that many of the viruses infecting us today have been in existence for millions of years (Stadnytskyi et al., 2020). Since the first vertebrates evoled, viruses have been multiplying and diversifying, eventually becoming the influenza viruses that today kill millions of people globally. In the early twentieth century, Spanish Flu alone caused nearly fifty million deaths, constituting the most devastating natural disaster in human history (Trilla et al., 2008). In recent years, Ebola, SARS, MERS, and Swine flu combined have killed tens of thousands of people globally (Trilla et al., 2008; Wong et al., 2015). Today, the coronavirus and the disease it causes (COVID-19) pose a threat to health security around the world and has already

* Corresponding author.
E-mail address: jjyoh@snu.ac.kr (J.J. Yoh).

https://doi.org/10.1016/j.scitotenv.2020.144725
0048-9697/

taken more than a million lives. With an estimated number of 10 nonillions (10^{13}) viruses on Earth, it is likely only a matter of time before another influenza virus containing human pathogens causes another global pandemic (Benvenuto et al., 2020; Nguyen et al., 2020), and the numbers above show the desperate need for improvement in virus diagnosis and detecting technologies. Therefore, this study attempts to develop a new technological procedure for measuring and determining the presence of viruses in real-time, airborne conditions.

The method for detecting the coronavirus is not very different from other virus detection methods. A typical coronavirus diagnosis involves reverse transcription polymerase chain reaction (RT-PCR) analysis of a mucus sample from the throat or nose. The sample is placed into a sterile container and transported to a lab where the virus RNA strands are transformed into DNA strands through RT. These DNA strands are then multiplied millions of times using PCR. These DNA strands are then detected using luminescent probes (Chen et al., 2020a; Chen et al., 2020b; Wang et al., 2020; Wang et al., 2020; Yuan et al., 2020). The process of testing an individual for COVID-19 has been vastly improved since the pandemic first began with test now producing results in a matter of minutes rather than days (Yuan et al., 2020). However, with scientists focusing on optimizing RT-PCR testing and checking individuals for infection, little consideration has been given to testing finite living spaces for the coronavirus.

Subsequently, there are currently no methods that allow determination of whether an enclosed space contains a concentrated amount of the coronavirus. However, developing such a tool is crucial to preventing the virus from spreading further. A preliminary report suggested that the chance of an infected person transmitting COVID-19 in an enclosed environment is 18.7-times greater than that in an open-air environment (Nishiura et al., 2020). Another recent study showed that in Wuhan hospitals, the coronavirus is most concentrated in enclosed toilet spaces whereas ventilated areas contain near-negligible amounts of the virus (Liu et al., 2020). Taken together, these two studies demonstrate the importance of developing a technology capable of instantaneous onsite monitoring of spaces for traces of the virus. Such technologies would help prevent people from unknowingly entering infected areas as well as aiding the development of more effective sanitization procedures. With such technology, only areas that test positive for the virus will need to be disinfected. Without it, as is currently the case, any space that has recently held a large number of people, such as classrooms and office spaces, are being disinfected with no knowledge of whether it is necessary, leading to resource and time wastage.

There are numerous studies on the spread of coronavirus in the air, the measurement of air quality in specific indoor areas, and coronavirus infection (Allen and Marr, 2020; Faridi et al., 2020; Kenarkoohi et al., 2020; Morawska and Cao, 2020; WHO, 2020; Stadnytskyi et al., 2020). Coronavirus infection caused by droplet propagation is known to be affected by humidity. Furthermore, numerous studies have demonstrated show how easily the virus spreads via large droplets in populated confined spaces (Allen and Marr, 2020; Morawska and Cao, 2020; Stadnytskyi et al., 2020). Studies have also revealed changes in coronavirus levels depending on the size of particulate matter (Bontempi, 2020; Comunian et al., 2020; Manoj et al., 2020; Shoor et al., 2020). This demonstrates that the flow of fine dust has a close relationship with coronavirus infection. There are also several studies on airborne infection by other viruses (D'Ancona et al., 2011; Lowen et al., 2007; Madewell et al., 2020; Niskanen and Lindberg, 2003). However, the current real-time detection methods for airborne viruses are not considered to be standardized diagnostic tests as they do not consider the propagation and concentration of a virus. Thus, airborne detection technologies are urgently required for identifying such viral outbreaks, airborne infections, chain infections, and unknown infections.

The detection of viruses using conventional Raman or IR spectroscopy is widely performed (Driskell et al., 2010; Fan et al., 2010; Khan and Rehman, 2020; Santos et al., 2020; Shanmukh et al., 2008; Roy et al., 2019; Tong et al., 2019; Wu et al., 2020) and demonstrates that it is possible to detect a spectral signal from a cultured virus specimen or one from the nasal munus of a person exposed to the virus after laser irradiation (Khan and Rehman, 2020). Furthermore, chemometrics and machine learning can be used for classifying laser spectra and identifying viruses using the specific spectral characteristics of viruses (Shanmukh et al., 2008). There have also been cases in which influenza A virus subtype H1N1 was detected by a biosensor technique called magnetic particle spectroscopy (Wu et al., 2020): which is a common biosensor-based virus detection method (Guliy et al., 2020; Nasrin et al., 2020; Seo et al., 2020; Zhang et al., 2020). The presence or absence of a virus can be confirmed from the concentration change of a virus after the biological reaction that occurs when a biosensor is exposed to a virus-containing environment (Guliy et al., 2020; Nasrin et al., 2020; Seo et al., 2020; Zhang et al., 2020). Plasma spectroscopy has also been used to identify the atomic signal of a virus-infected plants (Peng et al., 2017).

In this study, to monitor the air transmission and propagation of coronavirus, experiments were conducted using two fine powders ($Na_4C_6FeN_6 10H_2O$ and Na_2HPO_3), a synthetic protein antigen (SARS-CoV NP1), and a virus (Phix-174) that does not have a pathogen. These three types of samples (fine powder, antigen, and virus) are composed of phosphorus, carbon, nitrogen, and oxygen, which are atomic components similar to those of the coronavirus. Also, the Phix-174 virus has a similar size, shape, and molecular weight to those of coronavirus. Spark-induced plasma spectroscopy (SIPS), which has been proven effective for analyzing small particles in the air, is utilized. This technique generates plasma at a fixed location, even in the presence of air flow (Jung et al., 2020; Yang et al., 2020). Then, we investigated the changes in atomic signals with propagation distance and time in a chamber system. As a result, the main cause of air propagation and the concentration of airborne particles was identified as being related to measurement time and spray distance. It was inferred that there is a danger of droplet propagation via water droplets adsorbed onto objects. Real-time qualitative and quantitative analyses were also performed by detecting spectral bands for carbon, hydrogen, oxygen, and nitrogen, as well as several molecular bands, and nitrogen, all of which are characteristic of the Phix-174 virus. Accordingly, his study scientifically verifies a virus' ability to propagate when airborne by detecting the concentration of the virus in the air according to the movement of the virus when sprayed.

The purposes of this study can be summarized as follows: 1) to configure an experimental apparatus capable of real-time detection of covid-like viruses in ambient air; 2) to evaluate the effects of propagation distance and time; and 3) to perform real-time quantitative analysis on the specific components (carbon, hydrogen, oxygen, phosphorous, and molecules) of virus samples. Based on the results obtained, we have developed and verified a potential strategy for the detection of airborne viruses.

2. Material and methods

2.1. Sample preparation

In this study, three types of samples (fine powder, antigen, virus) were prepared in distilled water. The fine powders ($Na_4C_6FeN_6 10H_2O$ and Na_2HPO_3) comprise phosphorus, carbon, nitrogen, and oxygen, which are atom components similar to viruses, and were used at a concentration of 5 mM. The second sample was SARS CoV-2 NP1, which is an antigen of the coronavirus. This antigen was provided by BioNano Health Guard Research Center and subjected to real-time measurement of atomic carbon and sulfur. The third sample was the Phix174 virus, which was directly cultured before use and diluted as a concentration of up to 10,000 PFU/mL based on 1000 PFU/mL. In order to determine the exact concentration of the virus, a sample was purified before use.

Details of the purification procedure are given elsewhere (Kim et al., 2011).

The samples were sprayed using a nebulizer (OMRON, NE-C802) with the angle and amount sprayed held constant. We utilized the Phix174 virus because its size, shape, and molecular weight are similar to those of the coronavirus. The PhiX174 (ATCC 13706-B1), obtained from ATCC, was used as a surrogate of human enteric virus (Kim et al., 2020). Applying the plaque assay method (Kim et al., 2020), Phix174 was grown using *E. coli* host cells (ATCC 13706). To solidify the mixture, 0.2 mL of host cells, the serially diluted virus (0.1 mL), and 3 mL of soft agar containing 5 g/L of agar and 30 g/L of tryptic soy broth were added to tubes. The mixture was poured into tryptic soy agar plates and incubated at 37 °C for 18 h. The chemical information and representative atomic signals are shown in Table 1.

2.2. Chamber configuration

A 13 cm by 9 cm by 9 cm chamber was fabricated. There were two fans mounted inside the chamber to control air circulation. Inside the chamber, an aluminum base (1.5 cm by 2 cm) fixing two tungsten electrodes that generate spark-induced plasma was installed in the device. Holes with a diameter of 1 cm were drilled into both sides of the chamber so that the electrodes could be inserted. Qualitative and quantitative analysis was carried out by spraying the powder, antigen, or virus samples with a nebulizer inside the chamber or, for the powder samples, introducing it via air flow.

2.3. Spark-induced plasma (SIP) device

The SIPS system is illustrated in Fig. 1 and was used for the production of a spark via a high voltage discharge. The circuit for producing the spark-induced plasma consisted of a power supply (UltraVolt 6C24-P30, 6 kV, 90 mA) that provides very high DC voltages, two parallel-coupled high-voltage capacitors (HVCAP DMS HV capacitor, 0.1 μF, 30,000 Vdc) to preserve electrical power, a gap switch for providing electricity direction, a charging resistor, diodes, and a converter that facilitates electrical conversion from AC to DC. The spark-induced plasma was produced between a pair of tungsten electrodes with a purity of ≥99.8%. As shown in Fig. 1, a microcontroller (Arduino Uno R3) was utilized to (1) control the magnitude and frequency of the spark induced plasma and (2) connect with the ICCD system for maintaining a regular gate on timing. By measuring the charging and discharging time of the capacitor, the gate was opened after 1 μs based on the time when the discharge occurred, and the MCU was set to exclude the plasma continuum signal and obtain the plasma emission signal. For measuring plasma emission, we used an AR-coated focal lens (AC508-100-B, Thorlabs, focal length: 100 mm), an optical fiber (MF11, Thorlabs), and an ICCD camera (iStar, Andor). Spark-induced plasma was collected into the optic fiber, and the ICCD camera analyzed the emission line. In this research, the gate delay time was set from 1 to 2 μs and the width of the gate was set to 20 μs.

Table 1
Chemical information and representative peaks of samples.

Samples	Molecular information	Representative atomic information
Sample I (Powders)	Na_4 $C_6FeN_6 10H_2O$ Na_2 HPO_3	Na (588.99, 589.59 nm), C (247.86, 283.67, 283.76 nm), N (744.23, 746.83 nm), H (656.38 nm), O (777.19 nm), P (253.39, 255.53, 255.49 nm)
Sample II (SARS CoV2 NP1 antigen)	Nucleocapsid protein (N-protein), Spike protein (S-protein), ACE2	C (247.86, 283.67, 283.76 nm), S (545.38 nm), O (777.298 nm), H (656.3 nm), N (744.23, 746.83 nm), CN band (386.1–388.3 nm), C-C (516.2 nm)
Sample III (Phix-174)	Protein A, Protein A*, Protein B, Protein C, Protein D, Protein E, Protein F, Protein G, Protein H, Protein J, Protein K	C (247.86, 283.67, 283.76 nm), S (545.38 nm), O (777.298 nm), H (656.3 nm), N (744.23, 746.83 nm), CN band (386.1–388.3 nm), C-C (516.2 nm), P (253.39, 255.53, 255.49 nm)

2.4. Experimental environment to investigate the effects of distance and time

In this experiment, the concentration was precisely controlled. For the fine powders, 30 mL solution was used at a concentration of 5 mM; for the SARS CoV-2 NP1 antigen, a concentration of 1.6 mg/mL was used; and for the Phix174 virus, concentrations of 1000 to 10,000 PFU/mL were used. All samples were sprayed as droplets by a nebulizer (OMRON, NE-C802), and it was confirmed that 0.2–0.25 mL of liquid was emitted per spray, as shown in Fig. 1.

The amount of virus that can exist in a suspended state was tested in an ambient air conditions. In the case of the time experiments, since the spray distances were 4–10 cm, the atomic signals were detected at 5 cm. Measurements were made by comparing the intensity of the atomic signal present in the air based on the atomic signal detected for each sample. In this study, to ensure the stability of the signal, all of the data were averaged over 30 plasma emission signals while effectively minimizing fluctuations in the spectroscopic signal. The pertinent time to extract such data in an actual operating condition is <5 s.

3. Results and discussion

3.1. Sample I - effect of spray distance and measurement time for fine powder samples

The fine powder (<10 μm) were mixed with distilled water and sprayed with a nebulizer. As shown in Fig. 2, sodium, carbon, iron, nitrogen, hydrogen, oxygen, and phosphorus, which are the components of the powder, were detected. The signal to noise ratio (SNR) is >5000, and it can be seen that the plasma emission signal is measured stably. Fig. 2(a) and (c) is the results of increasing the sample transmitting distance to 5 to 25 cm, and Fig. 2(b) and (d) shows the effects of measurement time when the spray distance is fixed at 5 cm.

The changes in the signals for specific components with distance can be seen in Fig. 3(a–h). For powder 1 In powder 1(Na_4 $C_6FeN_6 10H_2O$), the atomic signals of sodium, carbon, iron, and nitrogen were tracked and measured from 5 to 30 cm at 5 cm intervals. These four elements have the highest atomic signal intensities, high SNRs, and relatively small deviations. In the case of powder 1, the signal intensity of sodium decreases as the distance increases. For carbon, when the distance increases from 5 to 10 cm, the signal intensity increases but decreases thereafter. There is a region in which the signal intensity of iron increases according to distance, but otherwise an overall decrease is observed. A gradual decrease in the signal intensity for nitrogen is observed.

For powder 2, the atomic signals for sodium, hydrogen, phosphorus, and oxygen were detected from 5 to 30 cm at 5 cm intervals. For sodium, the signal intensity decreases as the distance increases, and for hydrogen, the signal intensity increases when the distance increases from 15 to 20 cm, but the signal intensity otherwise decreases. There is a region in which the signal intensity of phosphorus increases with distance, but it tends to decrease, while the signal intensity of oxygen decreases with distance. The signal intensities of hydrogen and oxygen are quite high, which is likely due to the distilled water in which the powder is dissolved for the experiment. In addition, since the droplets are sprayed from a small nebulizer with a designed spray range of less than 30 cm, the arrival of droplets decreases with distance.

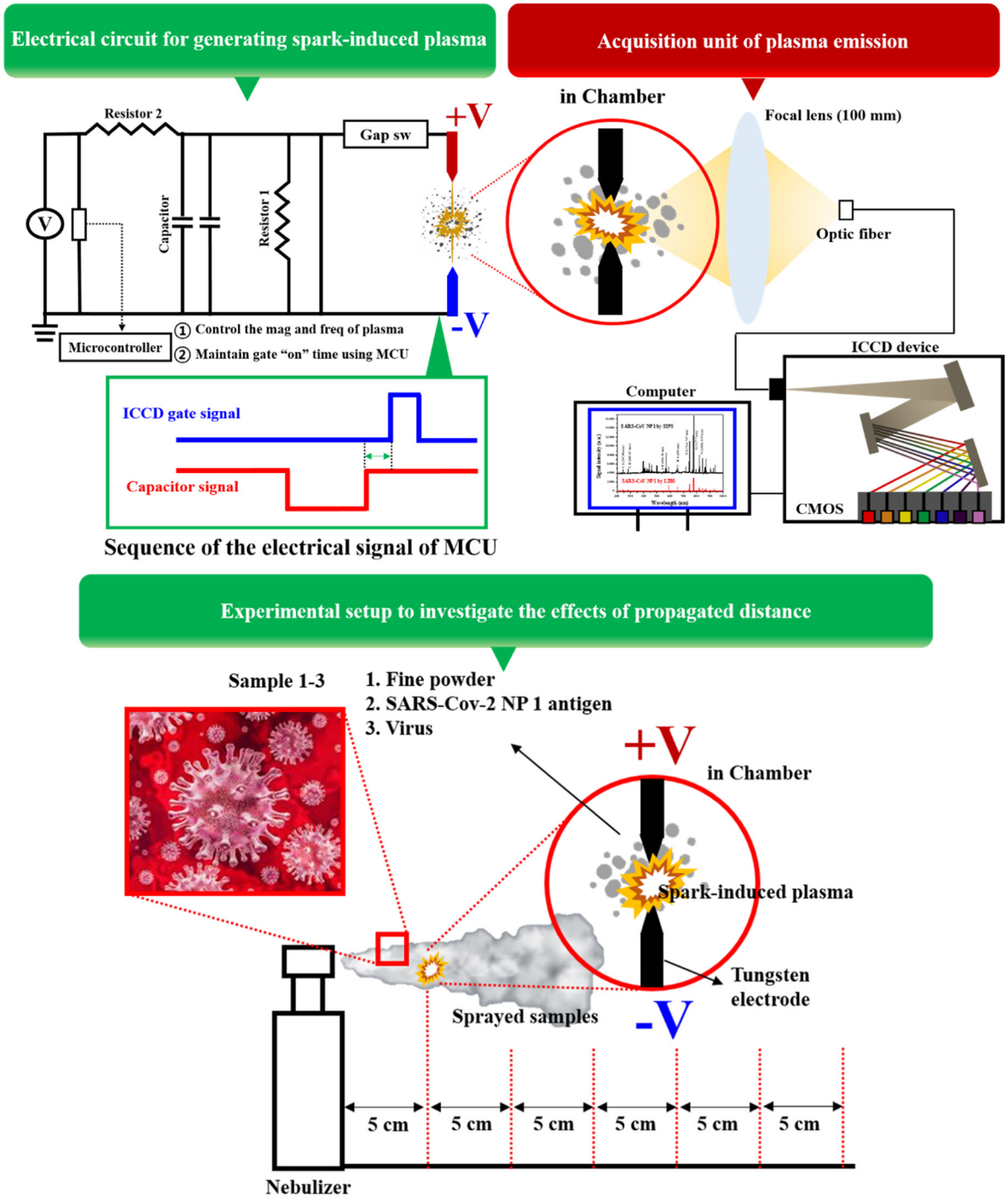

Fig. 1. Schematic of the SIPS system; electrical circuit and acquisition system for generating spark-induced plasma, and a schematic of the experimental setup used to investigate the effects of measurement distance and time.

Fig. 4(a) and (b) shows intensity changes for the atomic signals over measurement time at a fixed measurement distance of 5 cm. The results for nitrogen, sodium, and iron show that signal intensities decrease with measurement time in the same way as with distance. This is likely because when the powder is sprayed in the form of droplets, it is rapidly adsorbed onto the chamber surfaces rather than floating in the air. However, in the case of carbon, the signal intensity does not change significantly over time. This may be due to the low SNR for carbon. However, the final signal intensity for carbon is slightly lower than those after 5 and 0 s.

In the case of powder 2, the atomic signal intensities for sodium, hydrogen, phosphorus, and oxygen decrease over time. As discussed above, distilled water contains hydrogen and oxygen, but the decreases in their signals over time demonstrate that the distilled water does not exist in the floating state.

3.2. Sample II - effect of spray distance and measurement time for SARS CoV2 NP1 antigen

SARS-CoV2 NP1 is an artificial recombinant protein expressed in *E. coli*. It is composed of approximately 20 amino acids and thus assumed to comprise carbon, nitrogen, oxygen, hydrogen, and sulfur, which are the basic components of amino acids. We did not consider the signals for oxygen and hydrogen, as they are present in distilled

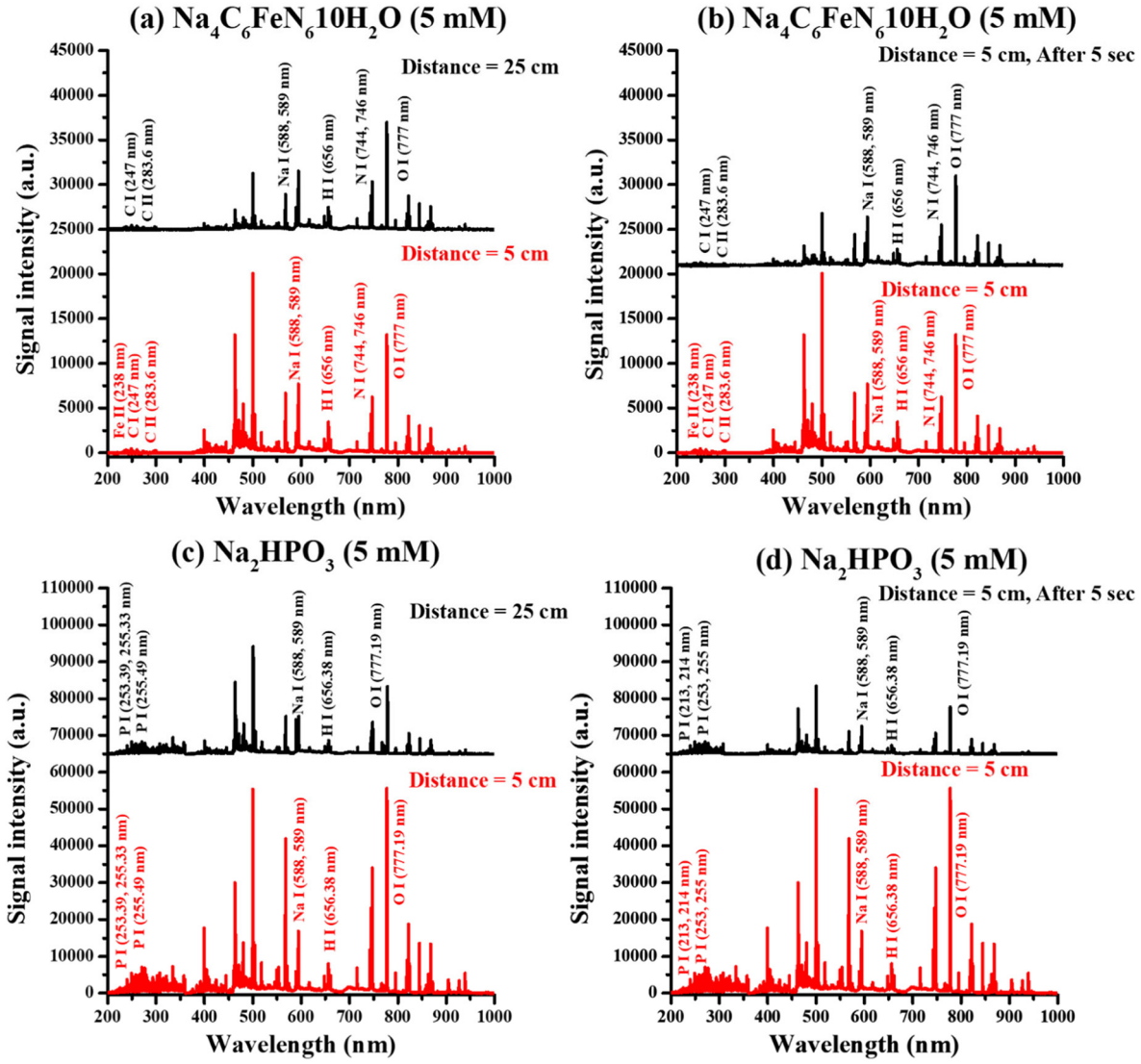

Fig. 2. Spectral changes according to spray distance and measurement time. (a) Signals for powder 1 ($Na_4C_6FeN_6 \cdot 10H_2O$) at spray distances of 5 and 25 cm; (b) signals for powder 1 ($Na_4C_6FeN_610H_2O$) at measurement times of 0 and 5 s; (c) signals for powder 2 (Na_2HPO_3) at spray distances of 5 and 25 cm; and (d) signals for powder 2 (Na_2HPO_3) for measurement times of 0 and 5 s.

water, or nitrogen, which is abundant in the air. As can be seen from Fig. 5, the SIPS spectrum of air only shows signals for nitrogen and oxygen, but that of airborne SARS-CoV NP1 shows signals for carbon and sulfur as well (as an increased hydrogen signal due to water).

Fig. 6(a–c) shows changes in carbon and sulfur signal intensities according to distance. The signal intensities decrease with distance from 5 to 30 cm. This shows that the SARS-CoV2 NP1 antigen is also highly restricted in its movement when sprayed in the droplet state, much like the powder samples. Thus, the antigen present in the droplets falls with the water in a short time and adsorbs to the floor or the side-walls of the measurement chamber. Furthermore, the amount of floating antigen decreases rapidly with distance. In the case of the sulfur signal, when the distance exceeds 20 cm, there is a slight increase in signal intensity, but this increase is within the error range.

Fig. 6(d–f) shows the changes in the signal intensity of carbon and sulfur according to measurement time after spraying. Clearly, the signals decrease with measurement time. When the SARS-CoV2 NP1 antigen is sprayed in the form of droplets, the large droplets fall rapidly and adsorb onto the chamber floor and do not float in the air. Some small droplets remain, but their density is much lower than that a measurement time of 0 s. It can be seen that the intensity decreases according to the plasma spectral signal (Eq. (1)) such that the signals of carbon and sulfur change according to the density of atoms.

$$I = FN_a^I A_{ul} \frac{g_u}{U_a^I} \exp\left(\frac{-E_u}{K_B T}\right) \quad (1)$$

Here,

I means the signal intensity of plasma emission, the experimental parameter is F, N_α^I means the number density of the chemical species at different ionization stages, the atomic number density indicating the transition probability is shown as A_{ul}, g_u and U_α^I are the upper-level degeneracy and the partition function at temperature T.

3.3. Sample III - effect of sprayed distance and measuring time for phix-174 virus

The virus concentration of all experiments in this section was maintained at around 5000 PFU (plaque forming units)/mL. As can be seen in Figs. 7 and 8, the chemical composition of the virus is slightly different from those of the powder and antigen samples. For instance, more intense molecular bands, such as CN and C-C bands, are observed. The

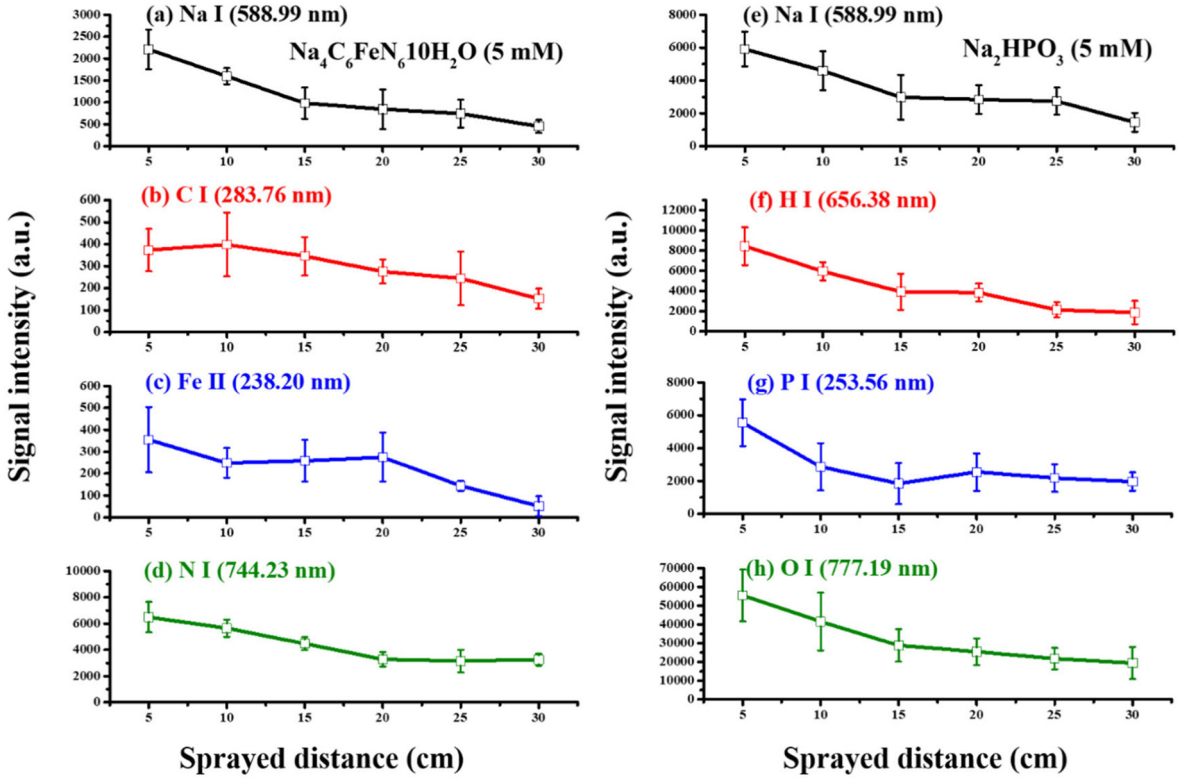

Fig. 3. Signal intensity changes for powder samples when the spray distance increases from 5 to 30 cm. (a-d) Sodium, carbon, iron, and nitrogen signals for powder 1; (e-h) sodium, hydrogen, phosphorus, and oxygen signals for powder 2.

CN band is a molecular signal detected in the presence of carbon and nitrogen under the conditions of Eqs. (2) to (5), and it presents its highest signal intensity at 388 nm (Mousavi et al., 2016).

$$C + N + M \rightarrow CN + M \quad (2)$$

$$C + N_2 \rightarrow CN + N \quad (3)$$

$$C_2 + N \rightarrow CN + C \quad (4)$$

The C-C band, it is a molecular band that occurs when two carbons are bonded together as in Eq. (5) (Mousavi et al., 2016).

$$C + C + M \rightarrow C_2 + M \quad (5)$$

In addition, it can be confirmed that the phosphorus signal, which indicates the genome, and the main components, carbon, nitrogen, hydrogen, and oxygen, are also present. When the distance is increased from 5 to 30 cm, the signal intensity gradually decreases, similar to the results for samples I and II. However, the signal for hydrogen does not decrease uniformly, which is likely due to the hydrogen in the water molecules present in the droplets. Considering that all signals except for hydrogen decrease with distance, and by considering Eq. (1), it can be concluded that the density of virus particles suspended in the air decreases rapidly with distance.

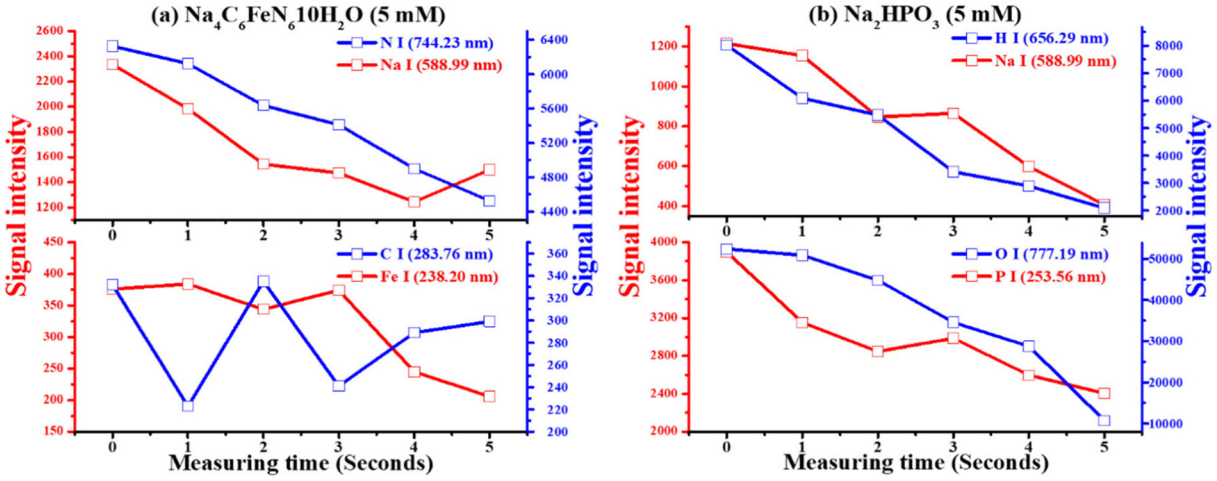

Fig. 4. Signal intensity changes for powder samples when measurement time was increased from 0 to 5 s. (a) Signal intensity changes for sodium, carbon, iron, and nitrogen in powder 1 ($Na_4C_6FeN_6 \cdot 10H_2O$), and (b) signal intensity changes for sodium, hydrogen, phosphorus, and oxygen in powder 2 (Na_2HPO_3).

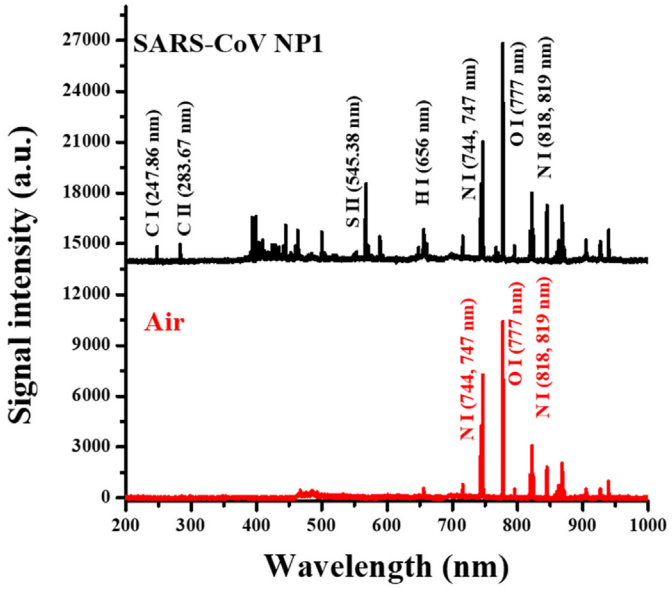

Fig. 5. Results obtained using SARS-CoV NP1. Comparison of the spectra for SARS-CoV NP1 and air.

Similarly, Fig. 9 shows the result when the measurement time is increased from 0 s to 5 s after the sample spraying (the results for hydrogen were not considered owing to the influence of water molecules). All the atomic signals gradually decrease. This indicates that the virus spray falls to the floor with the water and is adsorbed within a short 2–3 s time frame, just as for samples I and II. Therefore, it can be inferred that the spread of the virus adsorbed to surfaces is much more important than the spread of the virus in the air.

3.4. Construction of a calibration curve using the phix-174 virus for real-time quantitative analysis

In this study, quantitative analysis was conducted with the Phix-174 virus, which has a similar shape, molecular weight, and chemical composition to those of coronavirus. Hence, it can be considered a standard for the analysis of virus propagation and real-time analysis in air.

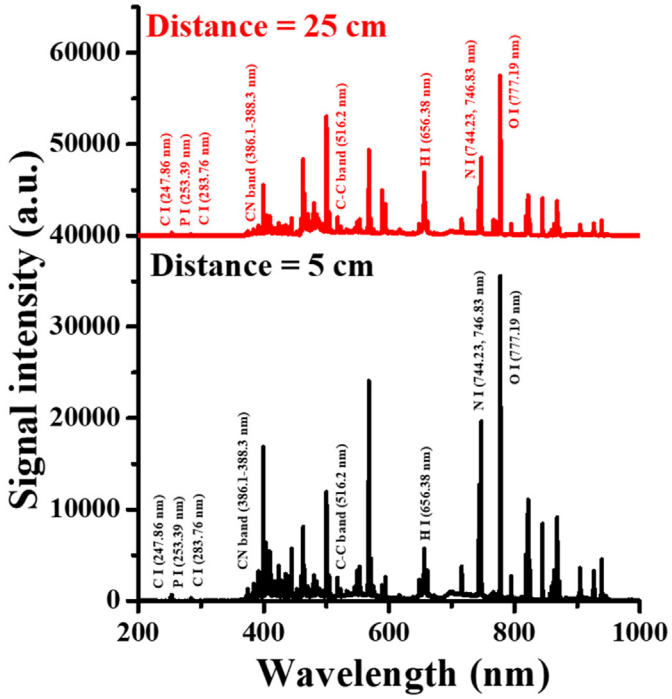

Fig. 7. Comparison of the spectra for Phix-174 at distances of 5 and 30 cm.

According to in Eq. (1), the intensities of the spectral signals change with virus concentration under the assumption that the temperature of the surrounding environment remains the same. The limit of detection (LOD) is derived from Eq. (6) using the correlation coefficient and standard deviation values and represents the lowest quantity of a substance that can be detected by the analytical method under investigation. In Eq. (6), S is the correlation between concentration and spectral signal intensity and σ_b is the standard deviation of the background. Therefore, the slope of the calibration curve is proportional to the LOD of the plasma spectroscopic method.

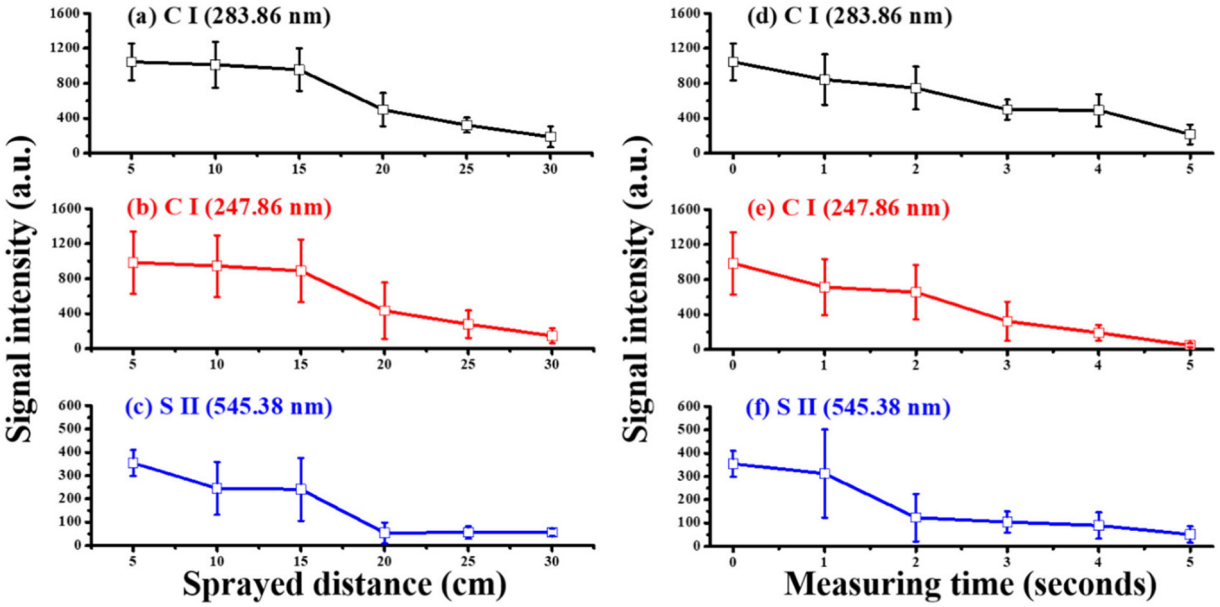

Fig. 6. Changes in signal intensities for SARS-CoV NP1 with spray distance and time. (a–c) Changes in carbon and sulfur signals for spray distances of 5 to 30 cm; (d–f) changes in carbon and sulfur signals for measurement times of 0 to 5 s.

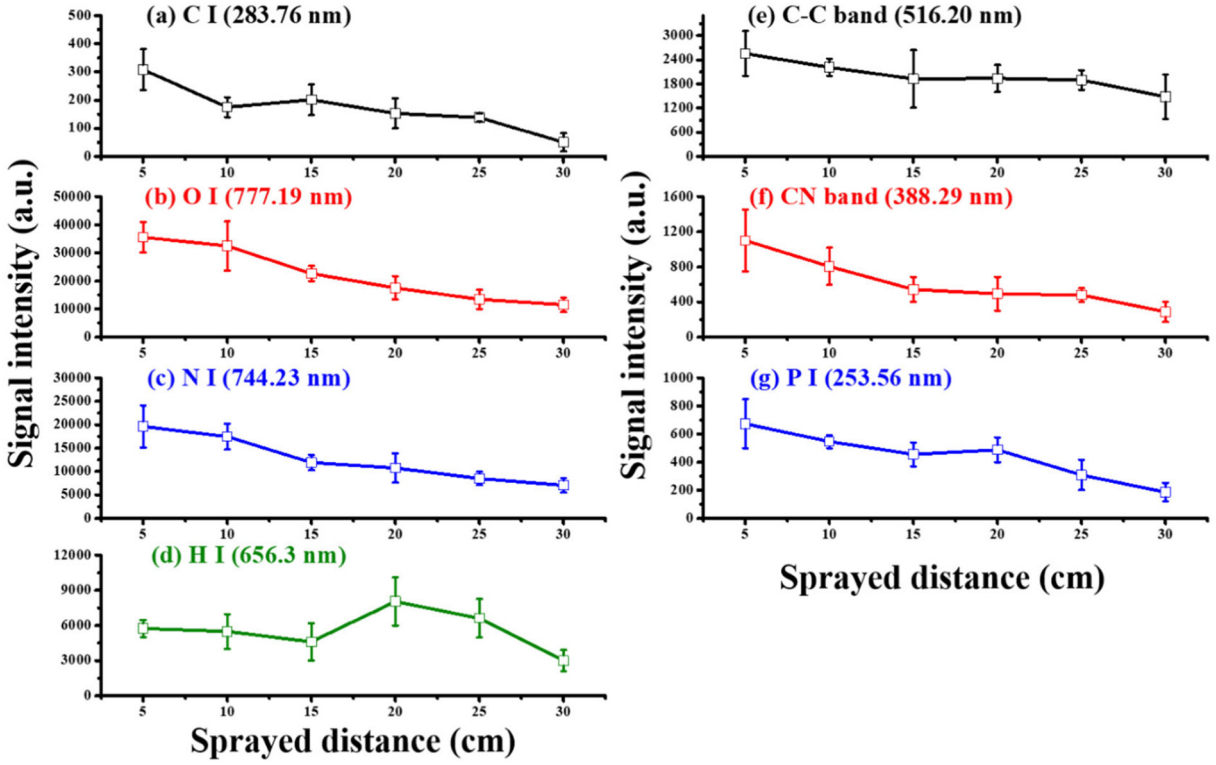

Fig. 8. Changes in signal intensities for the Phix-174 virus with spray distance from 5 to 30 cm. (a) Carbon I (283.76 nm), (b) oxygen I (777.23 nm), (c) C-C band (516.20 nm), (d) nitrogen I (744.23 nm), (e) hydrogen I (656.30 nm), (f) C-C band (516.20 nm), (g) CN band (388.29 nm), and (h) phosphorus I (253.56 nm).

$$LOD = \frac{3\sigma_b}{S} \tag{6}$$

Thus, by changing the concentration of Phix-174 in steps from 10,000 to 1000 PFU/mL, a calibration curve was constructed from the signals for carbon, nitrogen, C-C, CN, phosphorus, and oxygen. In all experiments in this section, the spraying distance was maintained at 5 cm and the measurement time was maintained at 0 s. As can be seen from Fig. 10, the system has LODs of approximately 1000 to 3000 PFU/mL depending on the signal considered. The R^2 values are distributed from 0.84 to 0.94, demonstrating that it is a model appropriate for linear regression analysis. The SIPS equipment used in this study can provide spectra within 3 s, and if there is a calibration curve as a reference, real-time quantitative analysis will be possible. Therefore, it was confirmed that SIPS provides real-time quantitative analysis of viruses

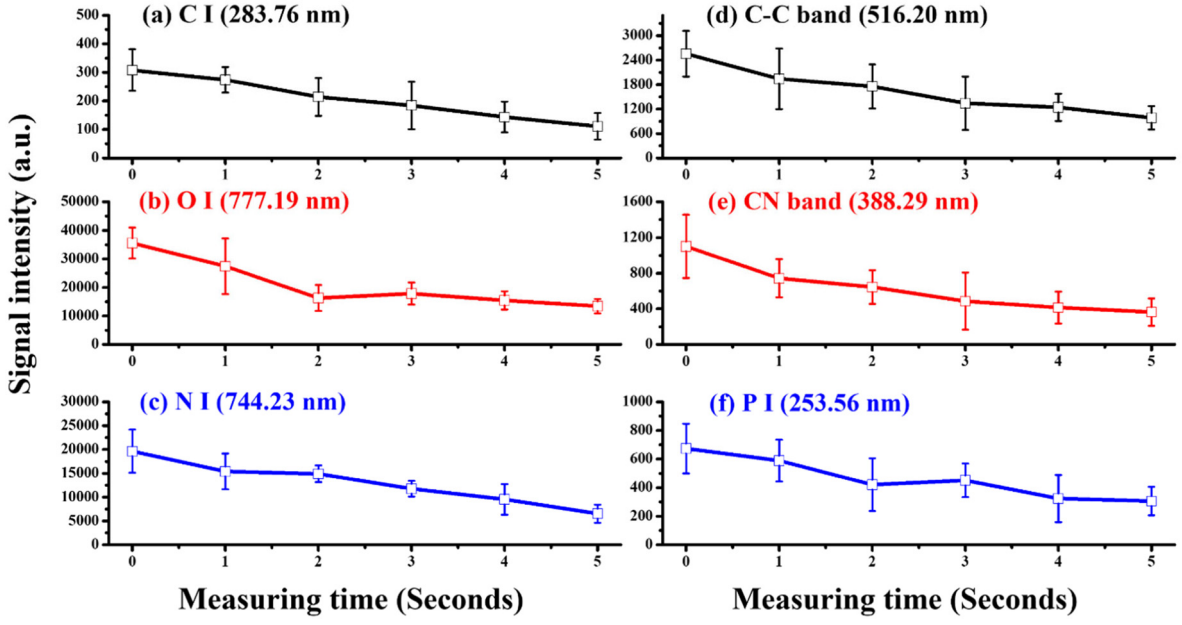

Fig. 9. Changes in signal intensities for the Phix-174 with measurement time from 0 to 5 s. (a) Carbon I (283.76 nm), (b) oxygen I (777.23 nm), (c) C-C band (516.20 nm), (d) nitrogen I (744.23 nm), (e) CN band (388.29 nm), and (f) phosphorus I (253.56 nm).

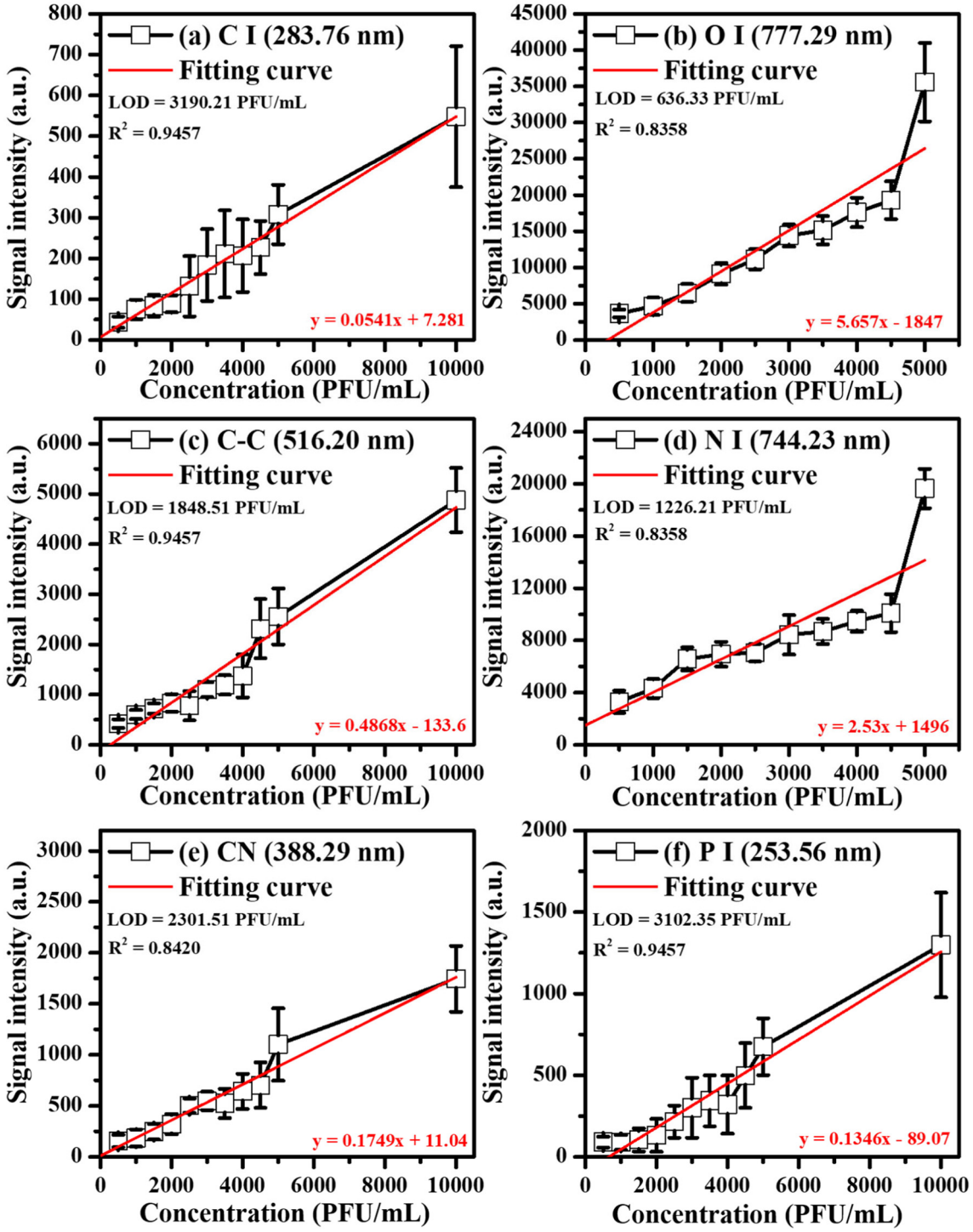

Fig. 10. Results of quantitative analysis using signal intensity changes for the Phix-174 virus. (a) Carbon I (283.76 nm), (b) oxygen I (777.23 nm), (c) C-C band (516.20 nm), (d) nitrogen I (744.23 nm), (e) CN band (388.29 nm), and (f) phosphorus I (253.56 nm).

floating in the air. Using Phix-174, spectral and distance results were derived.

4. Conclusion

This study was conducted to realize a system for real-time analysis of the spread and transmission of covid-like viruses in the air. This was performed by measuring the density of a virus floating in ambient air at different spray distances and measurement times using real-time SIPS analysis. As the measurement distance increased, the density of airborne powder, SARS-CoV2 NP1 antigen, and Phix-174 in water droplets significantly decreased. When the distance was increased to 30 cm, the signal intensity decreased more than 10-fold. The measurement time showed a similar trend as the measurement time was increased from 0 to 5 s. Thus, it can be assumed for coronavirus and other viruses that the risk of infection from droplets adsorbed on surfaces or the floor is higher. The danger of droplet propagation decreases with propagation time and distance.

Most importantly, our study shows that the apparatus developed can serve as a real-time quantitative detection platform with a LOD for

a virus of 1000 to 3000 PFU/mL and can determine particle concentration and the presence or absence of airborne coronavirus on site.

CRediT authorship contribution statement

J. Yang: Formal analysis, Investigation, Writing original draft. **J. Jung**: Investigation, Writing – review, **S. Kim** & **Y. Cho**: Sample preparation, **J. J. Yoh**: Conceptualization, Formal analysis, Writing – review & editing.

Declaration of competing interest

The authors declare that they have no known competing financial interests or personal relationships that could have appeared to influence the work reported in this paper.

Acknowledgments

This research was supported by the Samsung Research, Samsung Electronics Co., LTD., contracted through IAAT at Seoul National University.

References

Allen, J.G., Marr, L.C., 2020. Recognizing and controlling airborne transmission of SARS-CoV-2 in indoor environments. Indoor Air 30 (4), 557. https://doi.org/10.1111/ina.12697.

Benvenuto, D., Giovanetti, M., Ciccozzi, A., Spoto, S., Angeletti, S., Ciccozzi, M., 2020. The 2019-new coronavirus epidemic: evidence for virus evolution. J. Med. Virol. 92 (4), 455–459. https://doi.org/10.1002/jmv.25688.

Bontempi, E., 2020. First data analysis about possible COVID-19 virus airborne diffusion due to air particulate matter (PM): the case of Lombardy (Italy). Environ. Res., 109639 https://doi.org/10.1016/j.envres.2020.109639.

Chen, Y., Liu, Q., Guo, D., 2020a. Emerging coronaviruses: genome structure, replication, and pathogenesis. J. Med. Virol. 92 (4), 418–423. https://doi.org/10.1002/jmv.25681.

Chen, N., Zhou, M., Dong, X., Qu, J., Gong, F., Han, Y., Qiu, Y., Wang, J., Liu, Y., Wei, Y., Xia, J., Zhang, X., Zhang, L., 2020b. Epidemiological and clinical characteristics of 99 cases of 2019 novel coronavirus pneumonia in Wuhan, China: a descriptive study. Lancet 395 (10223), 507–513. https://doi.org/10.1016/S0140-6736(20)30211-7.

Comunian, S., Dongo, D., Milani, C., Palestini, P., 2020. Air pollution and Covid-19: the role of particulate matter in the spread and increase of covid-19's morbidity and mortality. Int J Env Res Pub He 17 (12), 4487. https://doi.org/10.3390/ijerph17124487.

D'Ancona, G., Capitanio, G., Chiaramonte, G., Serretta, R., Turrisi, M., Pilato, M., Arcadipane, A., 2011. Extracorporeal membrane oxygenator rescue and airborne transportation of patients with influenza A (H1N1) acute respiratory distress syndrome in a Mediterranean underserved area. Interact Cardiov Th 12 (6), 935–937. https://doi.org/10.1510/icvts.2010.260448.

Driskell, J.D., Zhu, Y., Kirkwood, C.D., Zhao, Y., Dluhy, R.A., Tripp, R.A., 2010. Rapid and sensitive detection of rotavirus molecular signatures using surface enhanced Raman spectroscopy. PLoS One 5 (4), e10222. https://doi.org/10.1371/journal.pone.0010222.

Fan, C., Hu, Z., Riley, L.K., Purdy, G.A., Mustapha, A., Lin, M., 2010. Detecting food-and waterborne viruses by surface-enhanced Raman spectroscopy. J. Food Sci. 75 (5), M302–M307. https://doi.org/10.1111/j.1750-3841.2010.01619.x.

Faridi, S., Niazi, S., Sadeghi, K., Naddafi, K., Yavarian, J., Shamsipour, M., Jandaghi, N.Z.S., Sadeghniiat, K., Nabizadeh, R., Yunesian, M., Momeniha, F., Mokamel, A., Hassanvand, M.S., MokjtariAzad, T., 2020. A field indoor air measurement of SARS-CoV-2 in the patient rooms of the largest hospital in Iran. Sci. Total Environ., 138401 https://doi.org/10.1016/j.scitotenv.2020.138401.

Guliy, O.I., Kanevskiy, M.V., Fomin, A.S., Staroverov, S.A., Bunin, V.D., 2020. Progress in the use of an electro-optical sensor for virus detection. Opt. Commun., 125605 https://doi.org/10.1016/j.optcom.2020.125605.

Jung, J., Yang, J.H., Yoh, J.J., 2020. An optimal configuration for spark-induced breakdown spectroscopy of bulk minerals aimed at planetary analysis. J. Anal. At. Spectrom. 35, 1103–1114. https://doi.org/10.1039/D0JA00057D.

Kenarkoohi, A., Noorimotlagh, Z., Falahi, S., Amarloei, A., Mirzaee, S.A., Pakzad, I., Bastani, E., 2020. Hospital indoor air quality monitoring for the detection of SARS-CoV-2 (COVID-19) virus. Sci. Total Environ., 141324 https://doi.org/10.1016/j.scitotenv.2020.141324.

Khan, R.S., Rehman, I.U., 2020. Spectroscopy as a tool for detection and monitoring of Corona Virus (COVID-19). Expert. Rev. Mol. Diagn. 20 (7), 647–649. https://doi.org/10.1080/14737159.2020.1766968.

Kim, J.Y., Lee, C., Love, D.C., Sedlak, D.L., Yoon, J., Nelson, K.L., 2011. Inactivation of MS2 coliphage by ferrous ion and zero-valent iron nanoparticles. Environ. Sci. Technol. 45 (16), 6978–6984. https://doi.org/10.1021/es201345y.

Kim, T., Cho, J., Cha, D., Kim, M.S., Park, E.J., Lee, H.J., Lee, C., 2020. Cupric ion in combination with hydrogen peroxide and hydroxylamine applied to inactivation of different microorganisms. J. Hazard. Mater. 400, 123305. https://doi.org/10.1016/j.jhazmat.2020.123305.

Liu, Y., Ning, Z., Chen, Y., Guo, M., Liu, Y., Gali, N.K., Duam, Y., Cai, J., Westerdahl, D., Liu, X., Ho, K., Kan, H., Fu, Q., Lan, K., 2020. Aerodynamic analysis of SARS-CoV-2 in two Wuhan hospitals. Nature 582 (7813), 557–560. https://doi.org/10.1038/s41586-020-2271-3.

Lowen, A.C., Mubareka, S., Steel, J., Palese, P., 2007. Influenza virus transmission is dependent on relative humidity and temperature. PLoS Pathog. 3 (10), e151. https://doi.org/10.1371/journal.ppat.0030151.

Madewell, Z.J., López, M.R., Espinosa-Bode, A., Brouwer, K.C., Sánchez, C.G., McCracken, J.P., 2020. Inverse association between dengue, chikungunya, and Zika virus infection and indicators of household air pollution in Santa Rosa, Guatemala: a case-control study, 2011-2018. PLoS One 15 (6), e0234399. https://doi.org/10.1371/journal.pone.0234399.

Manoj, M. G., Kumar, M. S., Valsaraj, K. T., Sivan, C., Vijayan, S. K., 2020. Potential link between compromised air quality and transmission of the novel corona virus (SARS-CoV-2) in affected areas. Environ. Res, 110001. doi:https://doi.org/10.1016/j.envres.2020.110001.

Morawska, L., Cao, J., 2020. Airborne transmission of SARS-CoV-2: the world should face the reality. Environ. Int., 105730 https://doi.org/10.1016/j.envint.2020.105730.

Mousavi, S.J., Farsani, M.H., Darbani, S.M.R., Mousaviazar, A., Soltanolkotabi, M., Majd, A.E., 2016. CN and C 2 vibrational spectra analysis in molecular LIBS of organic materials. Appl Phys B-Lasers O 122 (5), 106. https://doi.org/10.1007/s00340-016-6371-6.

Nasrin, F., Chowdhury, A.D., Takemura, K., Kozaki, I., Honda, H., Adegoke, O., Park, E.Y., 2020. Fluorometric virus detection platform using quantum dots-gold nanocomposites optimizing the linker length variation. Anal. Chim. Acta 148–157. https://doi.org/10.1016/j.aca.2020.02.039.

Nguyen, T.M., Zhang, Y., Pandolfi, P.P., 2020. Virus against virus: a potential treatment for 2019-nCov (SARS-CoV-2) and other RNA viruses. Cell Res. 30, 189–190. https://doi.org/10.1038/s41422-020-0290-0.

Nishiura, H., Oshitani, H., Kobayashi, T., Saito, T., Sunagawa, T., Matsui, T., Wakita, T., MHLW COVID-19 Response Team, Suzuki, M., 2020. Closed environments facilitate secondary transmission of coronavirus disease 2019 (COVID-19). MedRxiv. https://doi.org/10.1101/2020.02.28.20029272.

Niskanen, R., Lindberg, A., 2003. Transmission of bovine viral diarrhoea virus by unhygienic vaccination procedures, ambient air, and from contaminated pens. Vet. J. 165 (2), 125–130. https://doi.org/10.1016/S1090-0233(02)00161-2.

Peng, J., Song, K., Zhu, H., Kong, W., Liu, F., Shen, T., He, Y., 2017. Fast detection of tobacco mosaic virus infected tobacco using laser-induced breakdown spectroscopy. Sci. Rep. 7, 44551. https://doi.org/10.1038/srep44551.

Roy, S., Perez-Guaita, D., Bowden, S., Heraud, P., Wood, B.R., 2019. Spectroscopy goes viral: diagnosis of hepatitis B and C virus infection from human sera using ATR-FTIR spectroscopy. clin. Spectrosc 1, 100001. https://doi.org/10.1016/j.clispe.2020.100001.

Santos, M. C., Morais, C. L., Lima, K. M., 2020. ATR-FTIR spectroscopy for virus identification: a powerful alternative. Biomed Spectrosc Imaging, (Preprint), 1–16. doi: https://doi.org/10.3233/BSI-200203.

Seo, G., Lee, G., Kim, M.J., Baek, S.H., Choi, M., Ku, K.B., Lee, C., Jun, S., Park, D., Kim, H.G., Kim, S., Lee, J., Kim, B.T., Park, E.C., Kim, S.I., 2020. Rapid detection of COVID-19 causative virus (SARS-CoV-2) in human nasopharyngeal swab specimens using field-effect transistor-based biosensor. ACS Nano 14 (4), 5135–5142. https://doi.org/10.1021/acsnano.0c02823.

Shanmukh, S., Jones, L., Zhao, Y.P., Driskell, J.D., Tripp, R.A., Dluhy, R.A., 2008. Identification and classification of respiratory syncytial virus (RSV) strains by surface-enhanced Raman spectroscopy and multivariate statistical techniques. Anal. Bioanal. Chem. 390 (6), 1551–1555. https://doi.org/10.1007/s00216-008-1851-0.

Shoor, P., Kaur, G. D., Chauhan, A. K., 2020. Atmospheric Conditions Affecting the Transmission of Covid-19 Virus. doi:10.20944/preprints202005.0467.v1.

Stadnytskyi, V., Bax, C.E., Bax, A., Anfinrud, P., 2020. The airborne lifetime of small speech droplets and their potential importance in SARS-CoV-2 transmission. Proc. Natl. Acad. Sci. U. S. A. 117 (22), 11875–11877. https://doi.org/10.1073/pnas.2006874117.

Tong, D., Chen, C., Zhang, J., Lv, G., Zheng, X., Zhang, Z., Lv, X., 2019. Application of Raman spectroscopy in the detection of hepatitis B virus infection. Photodiagn Photodyn 28, 248–252. https://doi.org/10.1016/j.pdpdt.2019.08.006.

Trilla, A., Trilla, G., Daer, C., 2008. The 1918 "Spanish flu" in Spain. Clin. Infect. Dis. 47 (5), 668–673. https://doi.org/10.1086/590567.

Wang, Y., Wang, Y., Chen, Y., Qin, Q., 2020. Unique epidemiological and clinical features of the emerging 2019 novel coronavirus pneumonia (COVID-19) implicate special control measures. J. Med. Virol. 92 (6), 568–576. https://doi.org/10.1002/jmv.25748.

Wong, G., Liu, W., Liu, Y., Zhou, B., Bi, Y., Gao, G.F., 2015. MERS, SARS, and Ebola: the role of super-spreaders in infectious disease. Cell Host Microbe 18 (4), 398–401. https://doi.org/10.1016/j.chom.2015.09.013.

World Health Organization., 2020. Modes of transmission of virus causing COVID-19: implications for IPC precaution recommendations: scientific brief, 27 March 2020 (No. WHO/2019-nCoV/Sci_Brief/Transmission_modes/2020.1). World Health Organization.

Wu, K., Liu, J., Saha, R., Su, D., Krishna, V.D., Cheeran, M.C.J., Wang, J.P., 2020. Magnetic particle spectroscopy for detection of influenza A virus subtype H1N1. ACS Appl Mater Inter 12 (12), 13686–13697. https://doi.org/10.1021/acsami.0c00815.

Yang, J.H., Jung, J., Ryu, J.H., Yoh, J.J., 2020. Real-time monitoring of toxic components from fine dust air pollutant samples by utilizing spark-induced plasma spectroscopy. Chemosphere 20, 127237. https://doi.org/10.1016/j.chemosphere.2020.127237.

Yuan, X., Yang, C., He, Q., Chen, J., Yu, D., Li, J., Zhai, S., Qin, Z., Du, K., Chu, Z., Qin, P., 2020. Current and perspective diagnostic techniques for COVID-19. ACS Infect. Dis. https://doi.org/10.1021/acsinfecdis.0c00365.

Zhang, Y., Odiwuor, N., Xiong, J., Sun, L., Nyaruaba, R.O., Wei, H., Tanner, N.A., 2020. Rapid molecular detection of SARS-CoV-2 (COVID-19) virus RNA using colorimetric LAMP. MedRxiv. https://doi.org/10.1101/2020.02.26.20028373.